We are IntechOpen, the world's leading publisher of Open Access books Built by scientists, for scientists

4,800
Open access books available

122,000
International authors and editors

135M
Downloads

Our authors are among the

154
Countries delivered to

TOP 1%
most cited scientists

12.2%
Contributors from top 500 universities

CLARIVATE ANALYTICS BOOK CITATION INDEX INDEXED

WEB OF SCIENCE™

Selection of our books indexed in the Book Citation Index in Web of Science™ Core Collection (BKCI)

Interested in publishing with us?
Contact book.department@intechopen.com

Numbers displayed above are based on latest data collected.
For more information visit www.intechopen.com

13

Electronic and Magnetic Properties of the Graphene-Ferromagnet Interfaces: Theory vs. Experiment

Elena Voloshina[1] and Yuriy Dedkov[2]
[1]*Physikalische und Theoretische Chemie, Freie Universität Berlin*
[2]*Fritz-Haber-Institut der Max-Planck-Gesellschaft, Berlin*
Germany

1. Introduction

Graphene is a two-dimensional sheet of carbon atoms arranged in a honeycomb lattice with two crystallographically equivalent atoms (C1 and C2) in the unit cell [Geim (2009); Geim & Novoselov (2007); Neto et al. (2009)] [Fig. 1(a)]. The sp^2 hybridization between one $2s$ orbital and two $2p$ orbitals leads to a trigonal planar structure with a formation of a σ bonds between carbon atoms that are separated by 1.42 Å. These corresponding σ bands have a filled shell and, hence, form a deep valence band. The half-filled $2p_z$ orbitals, which are perpendicular to the planar structure, form the bonding (π) and antibonding (π^*) bands in the electronic structure of graphene [Fig. 1(b)]. The π and π^* bands touch in a single point exactly at the Fermi energy (E_F) at the corner of the hexagonal graphene's Brillouin zone (K-points). Close to this so-called Dirac point (E_D) the bands display a linear dispersion and form perfect Dirac cones [Neto et al. (2009)] [Fig. 1(c)]. Thus, undoped graphene is a semimetal ("zero-gap semiconductor"). The linear dispersion of the bands mimics the physics of quasiparticles with zero mass, so-called Dirac fermions [Geim (2009); Geim & Novoselov (2007); Neto et al. (2009)].

The unique "zero-gap" electronic structure of graphene leads to some limitations for application of this material in real electronic devices. In order, for example, to prepare a practical transistor, one has to perform a "doping" of a graphene layer inducing electrons or holes in the electronic structure [Fig. 1(d)]. There are several ways of the modification of the electronic structure of graphene with the aim of doping. Among them are: (i) incorporation in its structure of nitrogen [Wang et al. (2009)] and/or boron [Dutta & Pati (2008)] or transition-metal atoms [Mao et al. (2008)]; (ii) using different substrates that influence the electronic structure of the graphene layer, e. g. metallic substrates for the graphene growth [Wintterlin & Bocquet (2009)]; (iii) intercalation of different materials underneath graphene grown on different substrates [Dedkov et al. (2008a; 2001); Enderlein et al. (2010); Gierz et al. (2008; 2010); Shikin et al. (2000)]; (iv) deposition of atoms or molecules on top [Boukhvalov & Katsnelson (2009); Coletti et al. (2010)]; etc.

The exceptional transport properties of graphene [Geim & Novoselov (2007)] make it a promising material for applications in microelectronics [Morozov et al. (2008); Novoselov et al. (2005)] and sensing [Schedin et al. (2007)]. This has recently led to a revival of interest

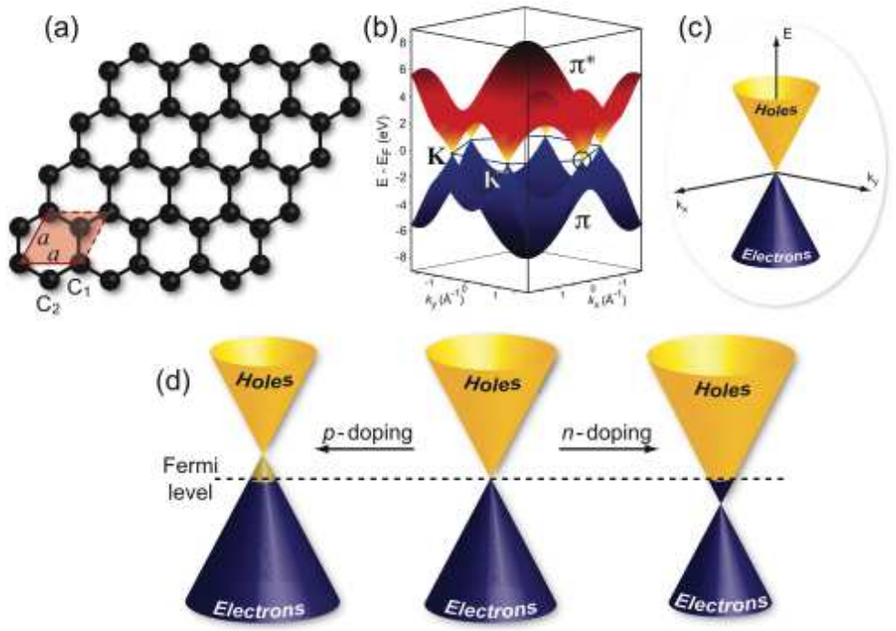

Fig. 1. (a) Crystal structure of the graphene layer where carbon atoms are arranged in the honeycomb lattice. Unit cell of graphene with lattice constant a has two carbon atoms per unit cell, C1 and C2. (b) Electronic dispersion of π and π^* states in the honeycomb lattice of free-standing graphene obtained in the framework of tight-binding approach. These branches have linear dispersion (c) in the vicinity of the K points of the Brillouin zone of graphene. (d) Position of the Dirac point and the Fermi level as a function of doping for the free-standing graphene.

in graphene on transition metal surfaces [Coraux et al. (2008; 2009); Dedkov et al. (2008a;b); Gamo et al. (1997); Hu et al. (1987); Land et al. (1992); Martoccia et al. (2008); N'Diaye et al. (2006); Sasaki et al. (2000); Sutter et al. (2009); Wang et al. (2008)], as large area epitaxial graphene layers of exceptional quality can be grown, which might be an alternative to micromechanical cleavage for producing macroscopic graphene films [Bae et al. (2010); Kim et al. (2029)].

The electronic interaction of graphene with a metal is both of fundamental and technological interest in view of possible device applications. Recent theoretical calculations by V. M. Karpan and co-workers [Karpan et al. (2007; 2008)] for graphene/metal interfaces imply the possibility of an ideal spin-filtering in the current-perpendicular-to-the-plane configuration (CPP) for the ferromagnet/graphene/ferromagnet sandwich-like structures. The close-packed surfaces of Co and Ni were considered as ferromagnetic (FM) electrodes, which perfectly coincide with graphene from the crystallographic point of view. The spin-filtering effect originates form the unique overlapping of the electronic structures of the graphene monolayer and close-packed surfaces of ferromagnetic Ni and Co. As discussed earlier, graphene is a semimetal with electronic density in the vicinity of E_F at corners (K points) of the hexagonal Brillouin zone of graphene. If the Fermi surface projections of ferromagnetic metals, fcc Ni or Co, on the (111) close-packed plane are considered, then in both cases one finds only minority electron density around the K points of the surface Brillouin zone. In this case, it is expected that the preferential transport of only minority electrons and

perfect spin-filtering will appear in a FM/graphene/FM stack [Karpan et al. (2007; 2008)], because graphene has electronic states only around K. The interaction between graphene and ferromagnetic material will however change the electronic properties of the interface partially quenching the spin-filtering effect in the sandwich-like structure, but a sizable effect can still be detected by choosing the proper combination of FM materials [Yazyev & Pasquarello (2009)] and this effect is predicted to increase strongly when multilayers of graphene are used [Karpan et al. (2007; 2008)].

Besides spin-filtering, graphene might be the best material for the realization of spintronic devices. Such systems usually require the effective injection of the spin-polarized electrons in the conductive channel which can be made from graphene [Tombros et al. (2007)]. However, prior to being able to implement graphene/ferromagnet systems in any kind of spintronic unit, a study of their electronic, magnetic, and interfacial properties has to be performed.

In the present chapter the electronic and magnetic structures of the graphene/FM interface will be discussed. From the theoretical side the different interfaces will be analyzed: graphene/Ni(111), graphene/Co(0001), graphene/1 ML Fe/Ni(111). Here the electronic structure of the interface as well as effect of induced magnetism in the graphene layer are discussed. As for experiment, the crystallographic structure, morphology, electronic and magnetic properties of a graphene/ferromagnet interface are considered for the case of the Ni(111) close-packed surface. Electronic structure studies of this interface reveal the existence of interface states, which originate from the strong hybridization of the graphene π and Ni $3d$ valence-band states leading to the appearance of the induced magnetic moment on the carbon atoms in the graphene layer that is confirmed by both x-ray magnetic circular dichroism (XMCD) and spin-resolved photoemission (PES). Detailed analysis of the Fermi surface of the graphene/Ni(111) system is performed via comparison of experimental and theoretical data for this interface.

2. Methods of investigations of graphene on ferromagnetic surfaces

2.1 Methods of calculation of the electronic and magnetic structure

Binding between graphene and metallic surface can be either chemical or physical in nature. Chemical binding typically implies a strong interaction through a charge sharing between the substrate and the adsorbate, yielding modification of their electronic structures. Physisorption, on the other hand, arises due to classical electrostatic or dispersion (van der Waals) interactions. The latter ones are the long-range correlation effects, which are not captured in the density functional theory (DFT) calculations because of the local character of standard functionals. In such cases, local density approximation (LDA) is known to give rather good results due to error cancellation. This is the reason of using for the graphene-containing systems the LDA, instead of generalized gradient approximation (GGA). Clearly, this is not a proper solution of the problem, and a better way would be to resort to methods beyond the DFT approach, either phenomenological or quantum-chemical post-Hartree-Fock correlation methods (see, e. g. [Paulus & Rosciszewski (2009); Pisani et al. (2008)]). An alternative approach is an inclusion of the dispersion correction to the total energy obtained with standard DFT approximation explicitly by hand with DFT-D method, that is atom pair-wise sum over C_6R^{-6} potentials (see, e. g. [Grimme (2004)]). High accuracy is accessible with a new exchange-correlation functional named van der Waals-density functional (vdW-DF), recently developed by Dion *et al.* [Dion et al. (2004)]. This functional is parameter free and therefore is considered *ab initio* in true spirit of DFT as it depends only on the total electron density.

The latter approach is shown to be working well for graphene/metal interface, where weak interaction between graphene and substrate is observed [Brako et al. (2010)].
In the previous theoretical studies on graphene/FM interface, the strong interaction for FM = Ni(111) or Co(0001) was found [Bertoni et al. (2005); Karpan et al. (2007; 2008)]. While existence of a non-magnetic configuration of graphene/Ni(111) interface, where graphene is weakly bound with substrate, was theoretically predicted, this structure was shown to be energetically unfavourable. The purpose of the present work is a comparison between theory and experiment, therefore the most stable configurations will be in the focus of the study. For them, standard GGA functionals are supposed to give reasonable result.
In our DFT studies, the electronic and structural properties of the graphene-substrate system are obtained using the Perdew-Burke-Ernzerhof (PBE) functional [Perdew et al. (1996)]. For solving the resulting Kohn-Sham equation we have used the Vienna Ab Initio Simulation Package (VASP) [Kresse & Furthmuller (1996a;b)] with the projector augmented wave basis sets [Blochl (1994)]. The plane-wave kinetic energy cutoff is set to 500 eV. The supercell used to model the graphene-metal interface is constructed from a slab of 13 layers of metal atoms with a graphene sheet adsorbed at both sides and a vacuum region of approximately 14 Å. When optimizing the geometry, the positions (z-coordinates) of the carbon atoms as well as those of the top two layers of metal atoms are allowed to relax. In the total energy calculations and during the structural relaxations the k-meshes for sampling the supercell Brillouin zone are chosen to be as dense as 24×24 and 12×12, respectively.

2.2 Experimental methods of investigation

The presented experimental studies of the graphene/Ni(111) interface were performed in different experimental stations in identical experimental conditions allowing for the reproducible sample quality in different experiments. In all experiments the W(110) single crystal was used as a substrate. Prior to preparation of the graphene/Ni(111) system the well-established cleaning procedure of the tungsten substrate was applied [Dedkov et al. (2008)]: several cycles of oxygen treatment with subsequent flashes to 2300°C. A well-ordered Ni(111) surface was prepared by thermal deposition of Ni films with a thickness of more than 200 Å on to a clean W(110) substrate and subsequent annealing at 300°C. An ordered graphene overlayer was prepared via thermal decomposition of propene (C_3H_6) according to the recipe described elsewhere [Dedkov et al. (2008;a;b; 2001); Nagashima et al. (1994)]. The quality, homogeneity, and cleanliness of the prepared graphene/Ni(111) system was verified by means of low-energy electron diffraction (LEED), scanning tunneling microscopy (STM), and core-level as well as valence-band photoemission.
STM experiments were carried out in an ultra-high vacuum (UHV) system (base pressure 8×10^{-11} mbar) equipped with an Omicron variable temperature scanning tunneling microscope. All STM measurements were performed in the constant-current-mode at room temperature using electrochemically etched polycrystalline tungsten tips cleaned in UHV by flash-annealing. The sign of the bias voltage corresponds to the voltage at the sample. Tunneling parameters are given separately for each STM image: U_T for tunneling voltage and I_T for tunneling current.
Near-edge absorption spectroscopy (NEXAFS) and XMCD spectra were collected at the D1011 beamline of the MAX-lab Synchrotron Facility (Lund, Sweden) at both Ni $L_{2,3}$ and C K absorption edges in partial (repulsive potential $U = -100$ V) and total electron yield modes (PEY and TEY, respectively) with an energy resolution of 80 meV. Magnetic dichroism spectra were obtained with circularly polarized light (degree of polarization is $P = 0.75$)

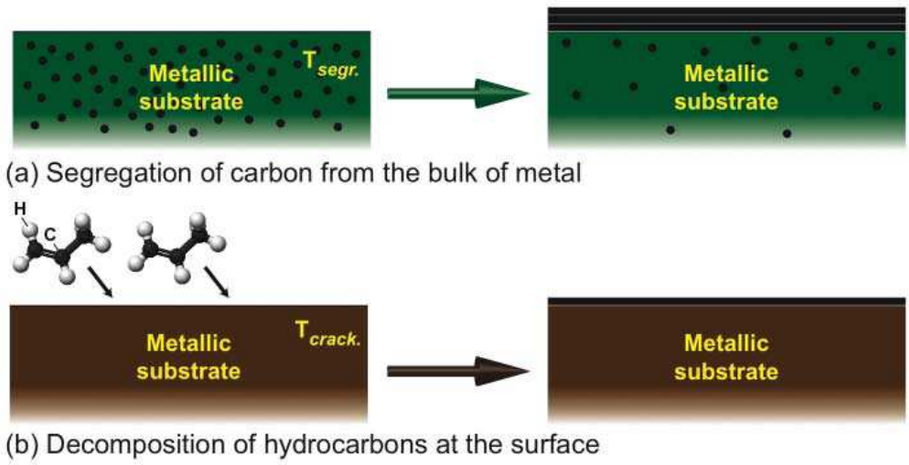

Fig. 2. Two ways of the graphene preparation on metal surfaces: (a) Segregation of bulk-dissolved carbon atoms to the surface at high temperature T_{segr}; (b) Decomposition (cracking) of hydrocarbon molecules at the surface of transition metals at high temperature T_{crack}.

in the remanence magnetic state of the graphene/Ni(111) system after applying of an external magnetic field of 500 Oe along the $< 1\bar{1}0 >$ easy magnetization axis of the Ni(111) film. All absorption measurements were performed at 300 K. The base pressure during the measurements did not exceed 1×10^{-10} mbar.
Angle-resolved PES (ARPES) experiments were performed at the UE56/2-PGM-1 beam-line at BESSY (Berlin, Germany). The photoemission intensity data sets $I(E, k_x, k_y)$ were collected with a PHOIBOS 100 energy analyzer (SPECS) while the graphene/Ni(111)/W(110) sample was placed on a 6-axes manipulator (3 translation and 3 rotation axes). The temperature of the sample during the measurements was kept at 80 K or 300 K. The energy/angular resolution was set to 80 meV/0.2°. In case of the spin-resolved PES experiments the mini-Mott-spin-detector (SPECS) was used instead of the 2D CCD detector. The spin-resolved spectra were collected in the remanent magnetic state of the graphene/Ni(111) system (see above) in normal emission geometry. The effective Sherman function was estimated to be $S_{eff} = 0.1$ and instrumental asymmetry was accounted via measuring of spin-resolved spectra for two opposite directions of the sample magnetization. The base pressure during all photoemission measurements was below 7×10^{-11} mbar.

3. Methods of graphene preparation on metallic surfaces

There are two common methods of the graphene preparation on metallic surfaces: (i) Segregation of the carbon atoms at the surface of bulk metallic sample, which was previously doped with carbon [Fig. 2(a)] and (ii) Decomposition of the carbon-containing molecules on the surface of transition metal [Fig. 2(b)]. In the first method the transition metal sample with some amount of carbon impurities or the bulk crystal, which was preliminary loaded by carbon (via keeping the sample at elevated temperature in the atmosphere of CO or hydrocarbons) is annealed at higher temperatures. This procedure leads to the segregation of carbon atoms at the surface of metal. The careful control of the temperature and the cooling rate of the sample allows to obtain the different thicknesses of the grown graphene layer: mono- vs. multilayer growth. In the second method the decomposition (cracking)

of carbon-containing molecules at the particular temperatures is used. Here, mostly light hydrocarbon molecules, like ethylene or propene, are used, but the decomposition of CO, acetylene, and of heavy hydrocarbon molecules, like cyclohexane, *n*-heptane, benzene, and toluene, also was successfully applied [Wintterlin & Bocquet (2009)]. In this method molecules could be adsorbed on the surface of metal at room temperature and then annealing of the sample leads to the molecule decomposition and hydrogen desorption; or molecules could be directly adsorbed on the hot sample. The recent experiments demonstrate that both methods, segregation and decomposition, practically lead to the graphene layers of the same quality. In case of segregation the kinetic of single graphene layer formation is defined by the careful controlling of the annealing temperature (but multilayers of graphene could be also prepared). In the second method the restriction to the formation of only single-layered graphene is defined by the fact that in this case the chemical reaction on the catalitically active metallic surface takes the place. Here the speed of hydrocarbon decomposition drops down by the several order of magnitude as soon the first grapehen monolayer is formed [Nagashima et al. (1994)]. List of metal surfaces, which were used for the preparation of graphene layers is compiled in Ref.[Wintterlin & Bocquet (2009)], where methods of preparation (segregation vs. decomposition), main experimental method, and corresponding reference are presented for different metallic surfaces (lattice-matched and lattice-mismatched).

4. Structure and bonding of graphene on ferromagnetic surfaces: Theory

The surface lattice constants of Ni(111), Co(0001), and the 1 ML Fe/Ni(111) system match the in-plane lattice constants of the graphene layer almost perfectly (compare: $a_{\mathrm{Ni}}/\sqrt{2} = 2.49$ Å, $a_{\mathrm{Co}} = 2.51$ Å, $a_{1\,\mathrm{ML\,Fe/Ni(111)}} = 2.52$ Å, and $a_{\mathrm{graphene}} = 2.46$ Å), that leads to the perfect crystallographic order at the interface between considered FM substrates and graphene. Several possible atomic configurations are usually considered for the interface between graphene and close-packed FM surface. Three "high-symmetry" structures, which preserve $3m$ symmetry, are known as $fcc-hcp$, $top-hcp$, and $top-fcc$. The latter one is schematically shown in Fig. 3: the C atoms are arranged above the Ni atoms of the first and third (fcc) layers. In the $top-hcp$ configuration, the C atoms are placed directly above the Ni atoms of the first layer (top site) and the second layer (hcp site). In the $fcc-hcp$ configuration, the C atoms are placed above fcc and hcp sites. Three additional configurations were considered recently, which were called $bridge-top$, $bridge-fcc$, and $bridge-hcp$. In these structures, one of the carbon atoms is not placed in top, fcc or hcp sites but in-between [Fuentes-Cabrera et al. (2008)].

In the present studies the electronic and magnetic structures of the graphene/Ni(111), graphene/Co(0001), and graphene/1 ML Fe/Ni(111) systems were calculated for the slab consisting of the graphene layer and 13 layers of FM material (in case of the latter system, 1 ML Fe was placed on the both sides of the 11-layers Ni slab in fcc stacking). As a first step the energy minimization for different structural arrangements of carbon atoms on FM surface was carried out. The results of these calculations are compiled in Table 1.

It has been found that the lowest energy configuration for FM = Ni or Co corresponds to a $top-fcc$ geometry in which one carbon atom is positioned above a surface FM atom (C-top) while the second carbon atom is situated above a third layer FM atom (C-fcc). This is in agreement with other previously published first-principles calculations [Bertoni et al. (2005); Eom et al. (2009); Karpan et al. (2007)] as well as with experiments for graphene on the Ni(111) surface [Gamo et al. (1997)]. In contrary to the latter result, where LEED $I-V$-curve analysis has been used in order to determine the interface arrangement, in experiments of C. Klink *et al.*

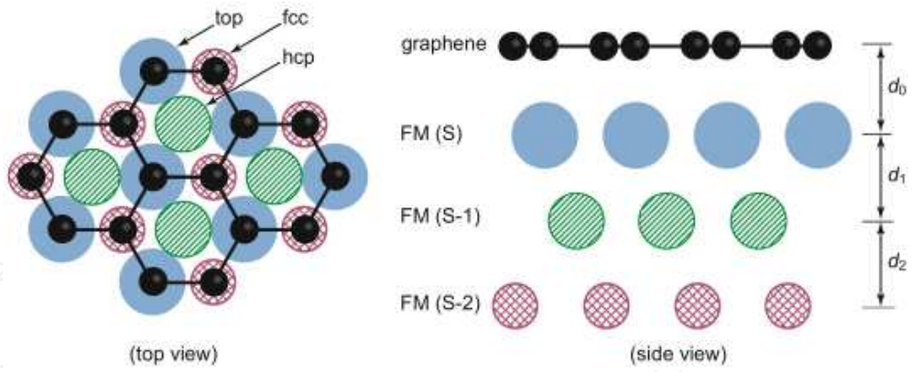

Fig. 3. Top- and side-view of a ball model of one of a possible arrangements of carbon atoms in a graphene layer on the lattice matched (111) surface. The different positions of carbon atoms in the graphene layer above FM interface atom (S) and on the hollow places above FM atoms in the second (S-1) as well as third layer (S-2) are marked as top, hcp, and fcc, respectively. d_{0-2} are distances between layers in the system.

[Klink et al. (1995)], involving combined STM and LEED studies, the $fcc-hcp$ configuration is shown to be the most stable one. The same conclusion was made by R. Rosei *et al.* [Rosei et al. (1983)], when using the extended-energy-loss fine-structure spectroscopy method. The calculations including three additional "low symmetry" configurations showed that within DFT employing GGA-PBE, none of the structures is stable at the experimentally relevant temperatures; with local-density approximation (LDA), the $bridge-top$ configuration was found to be the most energetically favorable one [Fuentes-Cabrera et al. (2008)].
The situation is different in the case of the graphene/1 ML Fe/Ni(111) system where the lowest-energy configuration was found to be $top-hcp$ with one carbon atom staying above Fe interface atom and the second one in the hollow hcp cite of the structure. The available experimental data [Dedkov et al. (2008a)] confirms the three-fold symmetry of this system, but cannot give any additional information about the stacking of the graphene and metallic layers. Structural studies by means of, e. g. LEED $I-V$-curve-analysis or x-ray diffraction, are necessary for this system.
The presented results (Table 1) demonstrate the reduction of the magnetic moment of the surface atoms of FM material upon adsorption of graphene on top. This reduction originates from the strong interaction between graphene π states and the 3d states of the FM interface layer. Such interaction leads to the noticeable modification of the graphene and metal valence band states, which will be discussed further in the text.
The electronic structure of a graphene sheet depends on its interaction strength with the ferromagnetic substrate. Clearly, the stronger bonding between graphene and underlaying metal, the shorter equilibrium distance d_0 between graphene and FM interface layer. As expected, this calculated distance is nearly the same for $top-fcc$ and $top-hcp$ arrangements, where one carbon atom of the graphene unit cell sits on top of a metal atom. But the energy difference found between these two models shows that FM atoms of the second and third layers also interact with the graphene layer. For the less strongly bound $fcc-hcp$ configurations of graphene on FM, the equilibrium separation is rather large, comparable to the layer spacing of 3.35 Å in bulk graphite (note: in our calculations, d_0 is slightly larger than can be expected due to the inability to describe dispersion interactions by PBE functional), indicating physisorption, and the characteristic band structure of an isolated graphene sheet is clearly recognizable.

	FM	Structure of the graphene/FM interface		
	Ni(111)	top-fcc	top-hcp	fcc-hcp
d_0 (Å)		2.135/2.133	2.145/2.146	3.540/3.540
d_1 (Å)	2.005	2.020	2.020	2.020
d_2 (Å)	2.031	2.017	2.015	2.036
ΔE (eV)		0.000	0.049	0.054
m_{FM} (μ_B)	−0.030/0.710	−0.025/0.543	−0.026/0.514	−0.029/0.669
m_{C} (μ_B)		−0.019/0.031	−0.019/0.027	0.000/0.000
	Co(0001)	top-fcc	top-hcp	fcc-hcp
d_0 (Å)		2.155/2.137	2.155/2.138	3.639/3.639
d_1 (Å)	1.954	1.963	1.956	1.952
d_2 (Å)	2.046	2.035	2.043	2.046
ΔE (eV)		0.000	0.017	0.090
m_{FM} (μ_B)	−0.053/1.784	−0.060/1.600	−0.059/1.583	−0.055/1.771
m_{C} (μ_B)		−0.043/0.038	−0.048/0.044	0.000/0.000
	1ML Fe/Ni(111)	top-fcc	top-hcp	fcc-hcp
d_0 (Å)		2.117/2.092	2.114/2.089	3.487/3.487
d_1 (Å)	2.039	2.029	2.019	2.028
d_2 (Å)	2.061	2.044	2.057	2.062
ΔE (eV)		0.021	0.000	0.104
m_{FM} (μ_B)	−0.028/2.622	−0.034/2.486	−0.035/2.469	−0.022/2.616
m_{C} (μ_B)		−0.048/0.040	−0.050/0.039	0.000/0.000

Table 1. Results for the atomic structure of the three graphene/FM interface models and for the clean FM surface: d_0 is the distance between the graphene overlayer and the interface FM layer (the two values for the two nonequivalent carbon atoms are indicated); d_1 is the distance between the interface FM layer and the second FM layer; d_2 is the distance between the second and third FM layers; ΔE is the energy difference between the energy calculated for the different slabs and the energy calculated for the most stable geometry; m_{FM} is the interface/surface FM spin magnetic moment (the two values for the sp and d magnetizations are indicated); m_{C} is the interface carbon spin magnetic moment (the two values for the two nonequivalent carbon atoms are indicated).

We consider the case of the graphene/Ni(111) as a representative one for the description of general features of the electronic structure of the graphene/FM interface with the analysis of the region around the Fermi level further in the text. The majority and minority spin band structures of the graphene/Ni(111) system (13 ML of Ni in the slab) with the $top-fcc$ arrangement of the carbon atoms are shown in Fig. 4. Due to the strong interaction between carbon layer and FM substrate, noticeable modification of the both graphene and FM band structure is observed. First of all, this is a nonrigid downward shift of the occupied graphene bands compare to those in pure graphene: at the Γ point, the π band is shifted by 2.25 eV while the σ band is only shifted by 1.15 eV. The unoccupied σ^* band is also shifted by 1.01eV. The interaction between graphene and metal layers implies a hybridisation of the graphene π bands with the nickel (cobalt, iron) $3d$ bands (and, in the second turn, with the FM $4s$ and $4p$ bands).

Strong hybridization of the graphene π and FM substrate $3d$ valence band states results in three occupied and two unoccupied hybridized states, with a strong contribution of the carbon p_z orbitals (see Fig. 5 for details). Four of them are clearly visible near the K point: $HS1$,

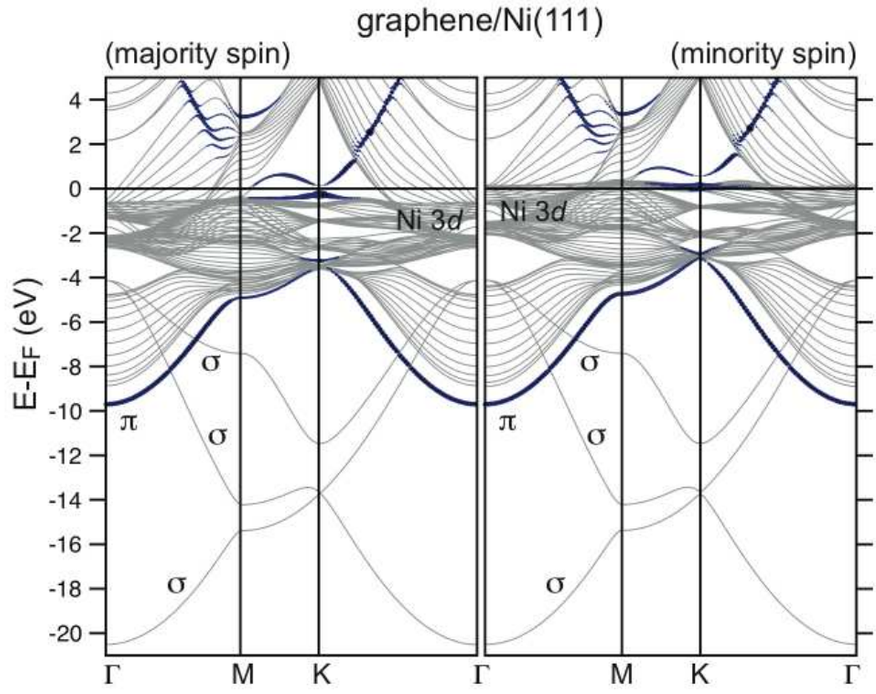

Fig. 4. Calculated majority and minority spin band structures for a slab terminated by graphene/Ni(111) interface for a most energetically favorable $top - fcc$ configuration. For the blue (darker) lines, the carbon p_z character is used as a weighting factor.

$HS2$, $HS3$, and $HS4$, respectively (Tab. 2). The states $HS2$ and $HS4$ can be attributed to the carbon atoms just above the interface nickel atoms, while the states $HS1$ and $HS3$ only involve the carbon atoms occupying the fcc hollow sites (Fig. 5). A 0.40 eV gap opening between the graphene occupied π and unoccupied π^* bands at the K point for the graphene/Ni(111) system is related to the $HS3$ and $HS4$. One more hybrid state $HS5$, observed near the M point of the Brillouin zone, results from a hybridisation of the interface nickel p_x, p_y, and d orbitals with carbon p_z orbitals (Fig. 5).

The resembling situation is observed for the graphene/Co(0001) and graphene/ 1 ML Fe/Ni(111) interfaces where similar hybridized states can be clearly identified in the calculated electronic structure (Fig. 5). The results of the analysis are summarized in Table 2. In the row Ni(111), Co(0001), 1 ML Fe/Ni(111) one can clearly identify increasing the exchange splitting between spin-up and spin-down counter-parts for every interface state, that can be assigned to increasing the magnetic moment of the underlying FM substrate. The interesting case is observed for graphene/1 ML Fe/Ni(111) where two Fe $3d$ quantum-well states of the minority character exist in the energy gap above the Fermi level around the K point [M. Weser, E.N.Voloshina, K.Horn, Yu.S.Dedkov (submitted)]. These states are strongly hybridized with C p_z states of C-top and C-hcp atoms that leads to increasing the magnetic moments of carbon atoms compared to those in the graphene/Ni(111) system (Table 1).

The calculated magnetic moment of the FM substrate for three systems, which are considered here are presented in Table 1. In all cases the deposition of the graphene layer on FM surface leads to the reduction of the magnetic moment of the interface FM atoms and appearing the induced magnetism of carbon atoms of graphene. For example, in the case of the most stable $top - fcc$ arrangement of the graphene/Ni(111) interface the magnetic moment of

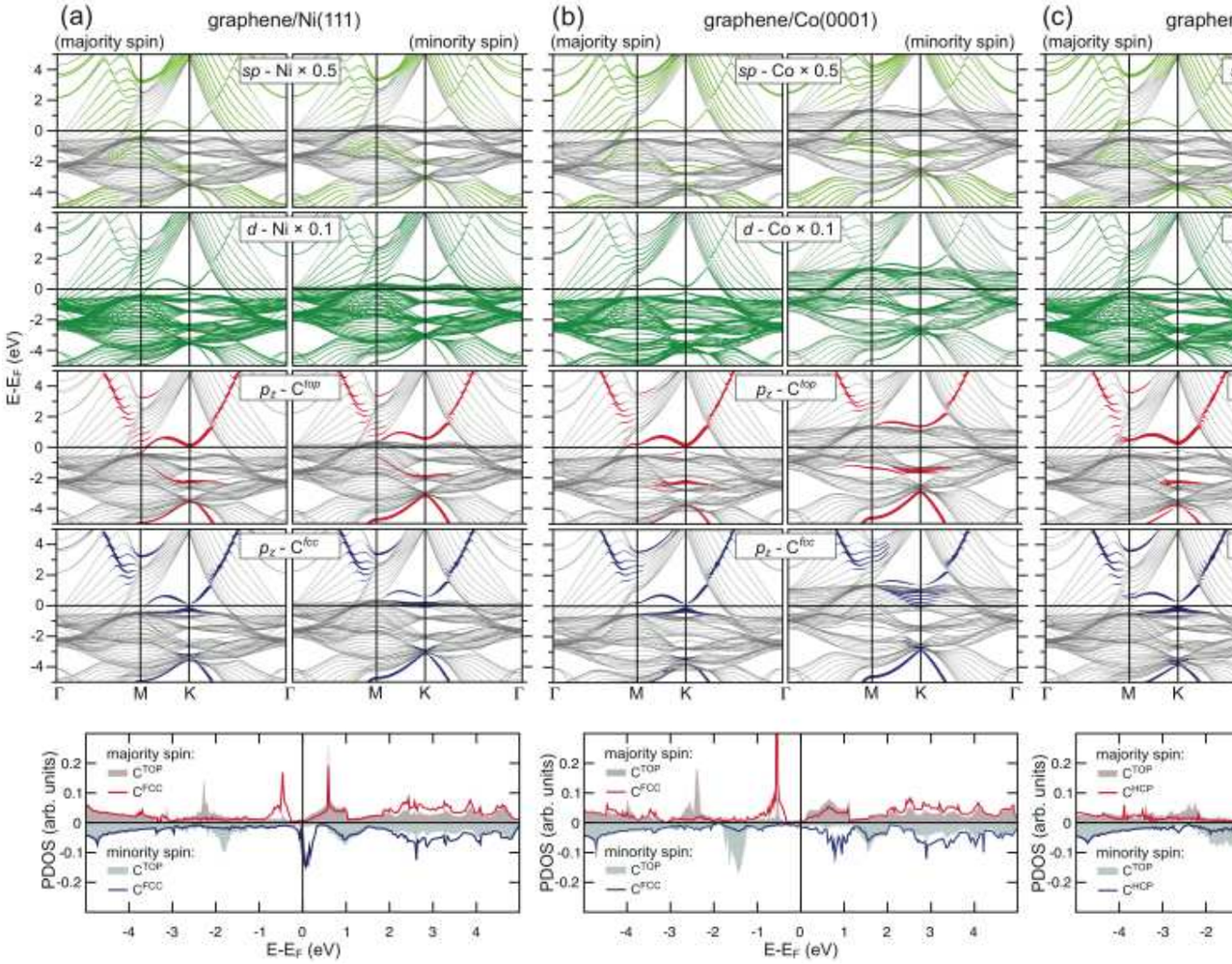

Fig. 5. Calculated majority and minority spin band structures for a slab terminated by: (a) graphen
fcc arrangement); (b) graphene/Co(0001) interfaces ($top - fcc$ arrangement); (c) graphene/1 ML Fe/N
arrangement). The radius of the circles is proportional to the partial density of states at the interface b
legend). The corresponding calculated majority and minority partial p_z density of states of graphene is
the lower panel of the figure.

State	FM = Ni(111)		FM = Co(0001)		FM = 1ML Fe/Ni(111)	
	spin ↑	spin ↓	spin ↑	spin ↓	spin ↑	spin ↓
$HS5$	−3.20	−3.32	−3.51	−4.01	−3.56	−4.05
$HS4$	−0.12	−0.55	−0.12	−1.27	−0.28	−1.72
$HS3$	0.28	−0.16	0.27	−0.95	0.26	−1.19
$HS2$	2.28	1.93	2.26	1.63	2.32	1.99
$HS1$	3.27	2.93	3.44	2.81	3.75	2.77

Table 2. Binding energies (in eV) (positive sign for states below the Fermi level and negative sign for states above the Fermi level) of the interface hybrid states (HS) extracted from the calculated band structures of the graphene/FM system at the K and M points (see text for details).

Ni interface atoms shows a reduction by about 20 % for $3d$ electrons. Our DFT calculations predict an induced magnetic moment of the carbon atoms in the graphene layer, which is equal to $-0.019\mu_B$ and $0.031\ \mu_B$ depending on the position of the carbon atom on the Ni(111) surface, due to the different behavior of the majority and minority spin interface states. The same behavior is also observed for the graphene/Co(0001) and graphene/1 ML Fe/Ni(111) interfaces where significantly large induced magnetic moments of carbon can be observed (Table 1).

5. Electronic and magnetic structure of graphene on ferromagnetic substrates: experiment

5.1 Growth and surface structure of graphene on Ni(111)

The quality of the samples at each preparation step was checked with LEED and STM. Since Ni(111) and graphene have the nearly similar lattice parameters (the lattice mismatch is of only 1.3 %), graphene forms the hexagonal (1×1) structure. Fig. 6(a) shows an overview of a graphene domain on Ni(111) after thermal decomposition of propene. The graphene layer is continuous and exhibits a highly ordered crystallographic structure without any visible defects even over large areas. Fig. 6(b) represents a magnified topographic image of the graphene lattice together with a typical LEED pattern of monolayer graphene on Ni(111) [inset of Fig. 6(b)]. A higher magnification STM image of the graphene surface is shown in Fig. 6(c) with the graphene hexagonal unit cell marked in the image.

So far several possible atomic configurations were considered for the graphene/Ni(111) intrface. Three "high-symmetry" structures are known as $hcp-fcc$, $top-hcp$, and $top-fcc$ and they are discussed in the previous section. In our case, graphene terraces have a peak-to-peak roughness of 0.2 Å and show a honeycomb structure with a lattice constant of 2.4 ± 0.1 Å [Fig. 6(b,c)], which agrees well with the expected 2.46 Å lattice spacing of graphene. STM images show that in the honeycomb unit cell carbon atoms corresponding to different sites appear with a different contrast, which can be attributed to the differences in the local stacking of the graphene sheet and the Ni(111) substrate. Therefore we interpret our STM images in the following way: Fig. 6 shows a single layer graphene, where carbon atoms most possibly occupy positions corresponding to one of the two non-equivalent configurations – $top-fcc$ or $top-hcp$. However, it turns to be impossible to directly identify which of the sites are occupied.

Additionally, some different orientations of the graphene relative to the Ni(111) substrate could be observed [Dedkov & Fonin (2010); Dedkov et al. (2008b)]. These observations show

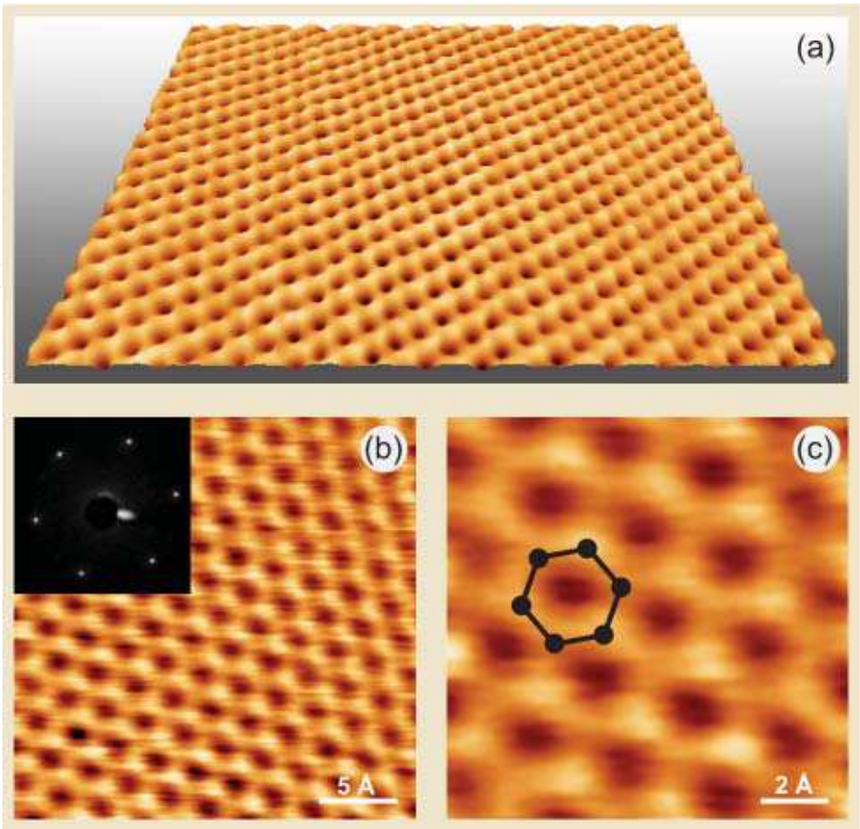

Fig. 6. High-quality graphene/Ni(111) system. (a) Large scale constant current STM image of the graphene/Ni(111) surface. Tunneling parameters: $U_T = 0.002\,\mathrm{V}$; $I_T = 48\,\mathrm{nA}$. (b) Magnified STM image of the perfect graphene lattice. The inset shows a LEED image obtained at 63 eV. (c) High magnification STM image showing atomic structure of the graphene monolayer. Tunneling parameters: $U_T = 0.002\,\mathrm{V}$; $I_T = 48\,\mathrm{nA}$. Graphene hexagonal unit cell is marked in (c).

that although the interaction between nickel and graphene is relatively strong, different adsorption geometries are locally possible.

5.2 Bonding and magnetism at the graphene/Ni(111) interface

In order to address the average spatial orientation of selected molecular orbitals (for example π or σ) at the graphene/Ni(111) interface, we vary the sample orientation with respect to the wave vector of the linearly polarized x-ray light and monitor the NEXAFS intensity. The observed changes of the NEXAFS lineshape at the C *K* edge in the graphene/Ni(111) system represent a nice example demonstrating the so-called *search-light*-like effect [Stöhr & Samant (1999)]. In such an experiment, the absorption intensity associated with a specific molecular orbital final state has a maximum if the electric field vector is aligned parallel to the direction of maximum charge or hole density, i. e. along a molecular orbital, and the intensity vanishes if the electric field vector is perpendicular to the orbital axis. The detailed description of the angular dependence of NEXAFS intensities can be found elsewhere [Stöhr (1999); Stöhr & Samant (1999)].

Figure 7 shows NEXAFS spectra of the graphene/Ni(111) system recorded at the C K absorption edge as a function of the angle, θ, between the direction of the incident linearly polarized x-ray light and the sample surface, e. g. between the electrical field vector of light and the sample surface normal (see the insets of Fig.7). The reference NEXAFS spectrum of the highly-oriented pyrolitic graphite (HOPG) crystal measured at $\theta = 30^\circ$ is shown in the upper part of the figure. The spectral features in the two broad regions $283 - 289$ eV and $289 - 295$ eV can be ascribed to C $1s \rightarrow \pi^*$ and C $1s \rightarrow \sigma^*$ transitions of core electrons into unoccupied states (π^*, σ_1^*, and σ_2^*), respectively. Upon the comparison of the NEXAFS C $1s \rightarrow \pi^*, \sigma^*$ spectrum of the graphene/Ni(111) system with the reference graphite spectrum, considerable changes in the spectral shapes are observed, which can be attributed to a strong chemisorption. A broadening of the π^* and σ^* resonances gives an evidence for a strong orbital mixing at the graphene/Ni interface, indicating a strong delocalization of the corresponding core-excited state. The characteristic double-peak structure at 285.5 and 287.1 eV can be qualitatively understood already with the ground-state DFT calculations (see present calculations discussed in the previous section and Ref. [Bertoni et al. (2005)]), while the dynamics of core-hole screening has to be considered for correct reproducing of the spectral profile [Rusz et al. (2010)]. In the ground-state approximation the first π^* resonance can be roughly associated with the unoccupied C $2p$ density of states located at the C atoms on top of Ni atoms, while the second π^* peak is mainly due to the C $2p$ density of states on the C atoms located at fcc hollow sites. However, in a real experiment individual contributions are considerably mixed and further affected by the core hole and its dynamical screening. The σ^* resonances are also influenced by the interaction with the substrate: they are visibly broadened and shifted by 0.6 eV to lower energies. The broadening is a result of the increased screening by the substrate electrons. The reduction of the $\pi^* - \sigma^*$ separation reflects the reduced anisotropy of the potential for outgoing electrons due to the slight ripple in the graphene layer on Ni(111) accompanied by a softening of the C-C bonds. A comparison of the present NEXAFS results for graphene on Ni(111) with those recently obtained for graphene/Rh and graphene/Ru [Preobrajenski et al. (2008)] indicates the existing of a very strong covalent interfacial bonding between carbon atoms in the graphene layer and Ni atoms of the substrate.

In the following we would like to compare our NEXAFS results with the recently calculated C K-edge electron energy-loss spectra (EELS) for the graphene/Ni(111) interface [Bertoni et al. (2005)]. In this case, experimental NEXAFS spectra taken at $\theta = 10^\circ$ and $\theta = 90^\circ$ correspond to the calculated EELS spectra for the scattering vector $\mathbf{q}$ perpendicular and parallel to the graphene layer, respectively. The calculated EELS spectra are found to agree well with the experimental NEXAFS data: (i) the spectra show the same angle (scattering vector) dependence and (ii) the experimentally observed NEXAFS features are well reproduced in the calculated EELS spectra. For example, two peaks in the NEXAFS spectra in the $1s \rightarrow \pi^*$ spectral region at 285.5 eV and 287.1 eV of photon energy can be assigned to the double-peak structure in the calculated EELS spectrum at 0.8 eV and 3.0 eV above the Fermi level [Bertoni et al. (2005)]. According to the theoretical calculations [Bertoni et al. (2005)], the first sharp feature in the NEXAFS spectrum is due to the transition of the electron from the $1s$ core level into the interface hybridized state HS_4 above the Fermi level (around the K point in the hexagonal Brillouin zone), which originates from the C p_z–Ni $3d$ hybridization and corresponds to the antibonding orbital between a carbon atom C-top and an interface Ni atom. The second peak in the NEXAFS spectrum is due to the dipole transition of an electron from the $1s$ core level into the interface hybrid state HS_5 above the Fermi level (around the M point in the hexagonal Brillouin zone), which originates from C p_z–Ni $p_x, p_y, 3d$ hybridization and

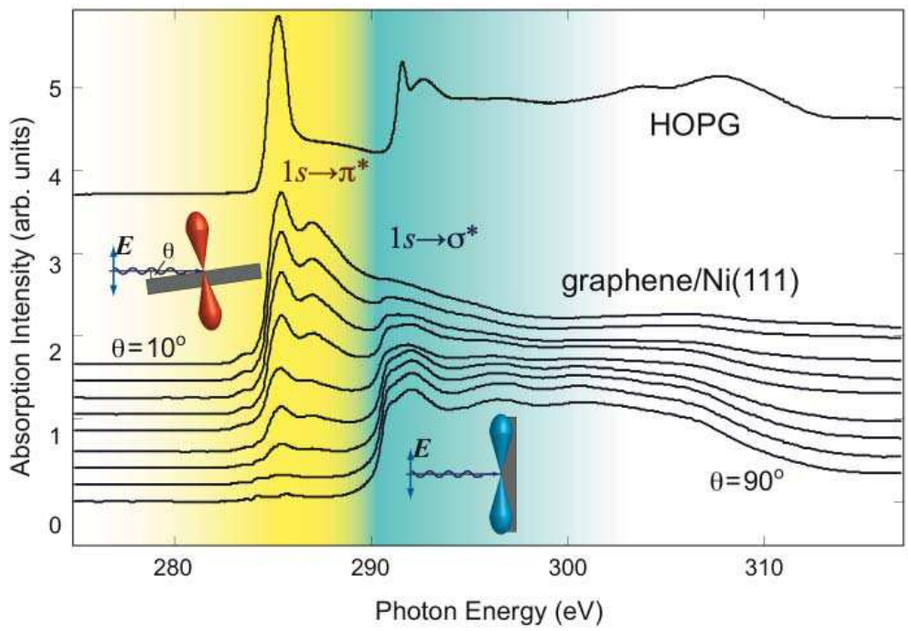

Fig. 7. Angular dependence of the absorption signal at the C *K* edge of the graphene/Ni(111) system measured as a function of angle, θ, between polarization vector of incoming linearly polarized light and the surface normal of the sample. Spectra were collected in the partial electron yield mode and angle was changed with a step of 10° from top to bottom. The reference spectrum of HOPG is shown in the upper part of the panel for comparison.

corresponds to a bonding orbital between C-*top* and C-*fcc* atoms, involving a Ni interface atom (see discussion about interface hybrid states in the previous section). In case of the NEXAFS C 1*s* $\rightarrow$ σ^*, the theory also correctly describes the shape of the absorption spectra [Bertoni et al. (2005)].

The strong hybridization between graphene π and Ni 3*d* valence band states at the graphene/Ni(111) interface leads to the partial charge transfer of the spin-polarized electrons from Ni onto C with the appearance of an induced effective magnetic moment of carbon atoms (Section 4), which can be detected in an experiment sensitive to the magnetic state of particular element, like XMCD. Figure 8 shows NEXAFS spectra of the graphene/Ni(111) system obtained for two opposite magnetization directions with respect to the polarization of the incident X-ray beam (upper panels) together with the resulting XMCD signal (lower panels). The spectra collected at the Ni $L_{2,3}$ edge in TEY mode and at the C *K* edge in PEY mode are presented in the left-hand panel and in the right-hand panel, respectively. The Ni $L_{2,3}$ XMCD spectrum (white line as well as fine structure behind the absorption edge) is in perfect agreement with previously published spectroscopic data [Dhesi et al. (1999); Nesvizhskii et al. (2000); Srivastava et al. (1998)]. The quantitative analysis of the absorption spectra obtained on a magnetic sample with circularly polarized light can be performed with the help of the so-called sum rules for spin- and orbital-magnetic moments [Carra et al. (1993); Thole et al. (1992)]. The intensities of L_3 and L_2 absorption lines and their differences for the parallel and anti-parallel orientations of the projection of photon spin on the sample magnetization direction are quantitatively related by the sum rules to the number of 3*d* holes in the valence band of the ferromagnetic material and the size of the spin and orbital magnetic moments.

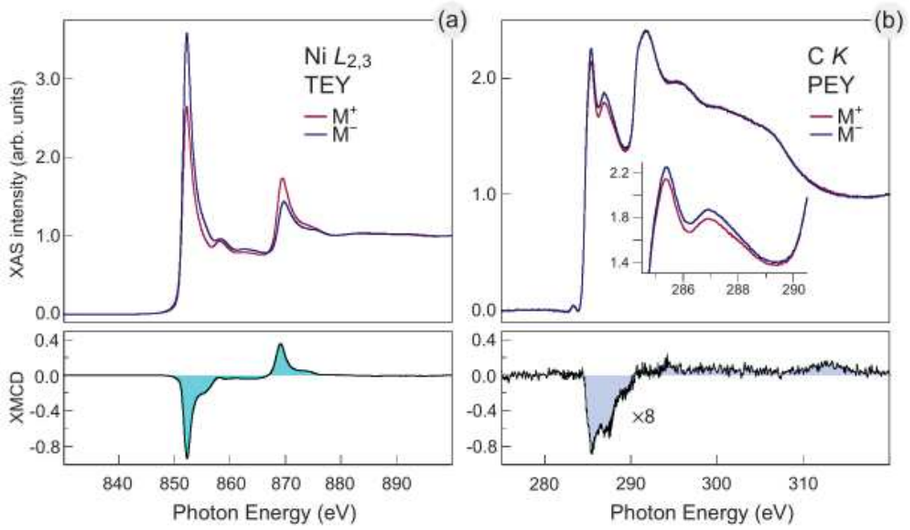

Fig. 8. XMCD spectra of the graphene/Ni(111) system: absorption spectra measured with circularly polarized light for two opposite orientations of the sample magnetization are shown in the upper part for the Ni $L_{2,3}$- (a) and C K-edges (b). The corresponding differences reflecting the strength of the dichroic signal are shown in the lower part of the respective figures.

From the experimental Ni $L_{2,3}$ TEY NEXAFS data [Fig. 8(a)] the bulk values of Ni 3d magnetic moments were derived, using a number of 3d holes in the valence band of Ni $n_h = 1.45$ [Sorg et al. (2004)] and polarization of light $P = 0.75$. At room temperature and in TEY mode (more bulk sensitive), Ni provides a spin moment of 3d electrons of $\mu_S = 0.69\,\mu_B$ and an orbital moment of $\mu_L = 0.07\,\mu_B$, respectively. These values coincide with the previously published experimental results [Baberschke (1996); Srivastava et al. (1998)]. The experimentally obtained spin-magnetic moment is very close to the calculated bulk value of $\mu_S = 0.67\,\mu_B$ for the graphene/Ni(111) system (Section 4). For the most energetically favorable configuration of carbon atoms on Ni(111), $top - fcc$, the calculations predict a reduction of the spin-magnetic moments of Ni interface atoms by 16 % down to $0.52\,\mu_B$ (Section 4). The experimental data collected at the Ni $L_{2,3}$ absorption edge in the PEY mode (more surface/interface sensitive) also shows a slight reduction of the spin moment to $\mu_S = 0.63\,\mu_B$. However, the observed decreasing is not so pronounced as yielded by the theoretical calculation, which can be explained by the large contribution of the bulk-derived signal to the XMCD spectra.
The most important and interesting results of these XMCD experiments on the graphene/Ni(111) system is the observation of the relatively large dichroic contrast at the C K absorption edge [Fig. 8(b)]. In order to magnify the measured magnetic contrast at the $1s \rightarrow \pi^*$ absorption edge, these XMCD spectra were collected in the PEY mode with the circularly polarized light at an angle of $\theta = 20°$. We note that the observed differences in the NEXAFS spectra collected at this angle visible in Figs. 7 and 8 are due to the different polarization of light: in Fig. 7(a) the data are obtained with the linearly polarized x-rays, i. e. the strong angular dependence of the absorption signal is due to the different graphene's orbital orientation; whereas the data in Fig. 8 are taken with the circularly polarized light, i. e. both $1s \rightarrow \pi^*$ and $1s \rightarrow \sigma^*$ transitions are nearly equivalently possible. The C K XMCD spectrum reveals that the major magnetic response stems from transitions of the $1s$ electron onto the π^*-states, while transitions onto the σ^*-states yield very weak (if any)

magnetic signal. These results indicate that only the C $2p_z$ orbitals of the graphene layer are magnetically polarized due to the hybridization with the Ni $3d$ band. The sharp structure at the $1s \rightarrow \pi^*$ absorption edge originates from hybridized C p_z–Ni $3d$ and C p_z–Ni p_x, p_y $3d$ states (see earlier discussion and Section 4).

The appearance of XMCD signal at the C K-edge shows that indeed the Ni film induces a magnetic moment in the graphene overlayer. However, at the C K absorption edge, the electron transitions occur from the non-spin-orbit split $1s$ initial states to the $2p$ final states and thus, in the analysis of the dichroism effect at the K edge one equation in the selection rules is missed. This means that the XMCD signal at K edges provides the information only on the orbital magnetic moment μ_{orb} [Carra et al. (1993); Huang et al. (2002); Thole et al. (1992)]. The partial charge transfer from Ni to C atoms in the graphene/Ni(111) system was calculated for the 22-atom (graphene)/Ni cluster [Yamamoto et al. (1992)] yielding $0.205e^-$ per C atom in graphene, which leads to the $2p$-orbital occupation number of $n_p = 2.205e^-$. Using the C K NEXAFS spectra the procedure described in work [Huang et al. (2002)], the orbital magnetic moment of $\mu_{orb} = 1.8 \pm 0.6 \times 10^{-3}\,\mu_B$ per C atom was extracted. The relatively large uncertainty arises mainly from the estimation of the number of C $2p$ holes, the background subtraction of NEXAFS spectra, and from the error for the degree of circular polarization of light.

The theoretical calculations presented in Section 4 also give the values for the spin magnetic moment of $-0.019\,\mu_B$ and $0.031\,\mu_B$ for C-top and C-fcc atoms, respectively. However, the magnetic splitting of the majority and minority parts of the interface hybrid states HS_3 and HS_4 was found between 0.44 and 0.43 eV, respectively, which may yield higher values for the magnetic moment. Due to the impossibility to directly extract the value of the spin magnetic moment form the K edge XMCD spectra, we apply a simple comparison with the magnetic measurements on similar systems in oder to estimate the average μ_S value for the carbon atoms at the graphene/Ni(111) interface. For the Fe/C multilayers clear magnetic signals of carbon were obtained by using the resonant magnetic reflectivity technique [Mertins et al. (2004)]. Hysteresis loop recorded at C K absorption edge gave a clear proof of ferromagnetism of carbon atoms at room temperature with a measured spin magnetic moment of $\mu_S = 0.05\,\mu_B$ induced by adjacent Fe atoms. The observed ferromagnetism of carbon in the Fe/C multilayered system was related to the hybridization between the Fe $3d$ orbitals and the C p_z orbitals, which are normal to the graphene-type layered sp^2-coordination. The second comparison can be performed with carbon nanotubes on ferromagnetic Co substrate [Céspedes et al. (2004)]. Carbon nanotubes were shown to become magnetized when they are in contact with magnetic material. Spin-polarized charge transfer at the interface between a flat ferromagnetic metal substrate and a multiwalled carbon nanotube leads to a spin transfer of about $0.1\,\mu_B$ per contact carbon atom. Additionally, a comparison of the XMCD spectra obtained at the C K edge in graphene/Ni(111) (present work) and at the O K edge in O/Ni(100) [Sorg et al. (2006)], reveals the approximately same magnitude of the XMCD signal. For the O/Ni(100) system, where the induced spin-magnetic moment of $0.053\,\mu_B$ on oxygen atom was calculated, the theoretically simulated NEXAFS and XMCD spectra agree well with the experimental data. Considering these analogous systems, we estimate the induced magnetic moment for graphene on Ni(111) to be in the range of 0.05-0.1 μ_B per carbon atom.

The experimentally observed effective magnetic moment of carbon atoms of the graphene layer on Ni(111) was recently confirmed by spin-resolved photoemission measurements [Dedkov & Fonin (2010)]. These data present the clear spin-contrast in the valence band region and a spin polarization value of about -60% at the Fermi level for the pure Ni(111)

surface. The presence of graphene on Ni(111) strongly modifies the valence band spectrum of Ni indicating the strong interaction between valence band states of graphene and Ni. In the graphene/Ni(111) system the spin polarization of Ni 3*d* states at E_F is strongly reduced to about -25%. The significant modifications of the spin-resolved structure of Ni 3*d* states as well as the reduction of the spin polarization at E_F is considered as an indication of decreasing the magnetic moment of Ni atoms at the graphene/Ni(111) interface. These spin-resolved photoemission measurements demonstrate the clear spin contrast for the graphene π states with the maximum spin-polarization of $P = -12 \pm 2\,\%$ at room temperature. The two spin-resolved π components are clearly resolved giving the exchange splitting of about 34 ± 9 meV for these states, which agrees well with the value extracted from theoretical calculations (Section 4).

5.3 Electronic properties of graphene on Ni(111)

Fig. 9(a) shows a series of angle-resolved photoemission spectra measured along the $\Gamma - \mathrm{K}$ direction of the hexagonal Brillouin zone of the graphene/Ni(111) system. This series is extracted from the 3D sets of data of photoemission intensity $I(E_B, k_x, k_y)$, where E_B is the binding energy and k_x, k_y are the orthogonal components of the in-plane wave vector. For the graphene/Ni(111) system the K and M points of the Brillouin zone are reached at $1.7\,\text{Å}^{-1}$ and at $1.4\,\text{Å}^{-1}$, respectively. The presented photoemission data are in very good agreement with previously published results [Dedkov et al. (2008b; 2001); Grüneis & Vyalikh (2008); Nagashima et al. (1994); Shikin et al. (2000)]. In Fig. 9(a) one can clearly discriminate dispersions of graphene π- and σ-derived states in the region below 2 eV of the binding energy (BE) as well as Ni 3*d*-derived states near E_F. The binding energy of the graphene π states in the center of the Brillouin zone (in the Γ point) equals to 10.1 eV which is approximately by 2.4 eV larger than the binding energy of these states in pure graphite. The shift to larger binding energy is different for σ and π valence band graphene-derived states. This behavior can be explained by the different hybridization strength between these states and Ni 3*d* valence band states, which is larger for the out-of-plane oriented π states compared with the one for the in-plane oriented σ states of the graphene layer as discussed in Section 4. The binding energy difference of ≈ 2.4 eV for the π states and ≈ 1 eV for the σ states between graphite and graphene on Ni(111) is in good agreement with previously reported experimental and theoretical values [Bertoni et al. (2005); Dedkov et al. (2008b)]. The effect of hybridization between Ni 3*d* and graphene π states can be clearly demonstarted in the region around the K point of the Brillouin zone: (i) one of the Ni 3*d* bands at 1.50 eV changes its binding energy by ≈ 150 meV to larger BE when approaching the K point; (ii) a hybridization shoulder is visible in photoemission spectra, which disperses from approximately 1.6 eV to the binding energy of the graphene π states at the K point [see also Fig. 9(b,c) for a detailed view]. The strong hybridization observed in PES spectra underlines the fact that the π states might become spin-polarized and might gain a non zero-magnetic moment due to charge transfer from the Ni atoms to the carbon atoms.

Considering the electronic band structure of the graphene/Ni(111), the region around the K point delivers the most interesting and important information with respect to the possible spin-filtering effects in the graphene/ferromagnet or ferromagnet/graphene/ferromagnet sandwich-like structures. This part of the electronic structure measured with two different photon energies ($h\nu = 70$ eV and 100 eV) is shown in Fig. 9(b,c) as color maps (upper panels) together with the corresponding intensity profiles directly at the K point (lower panels). Firstly, the spectral function of the graphene layer on Ni(111) is characterized by the absence of

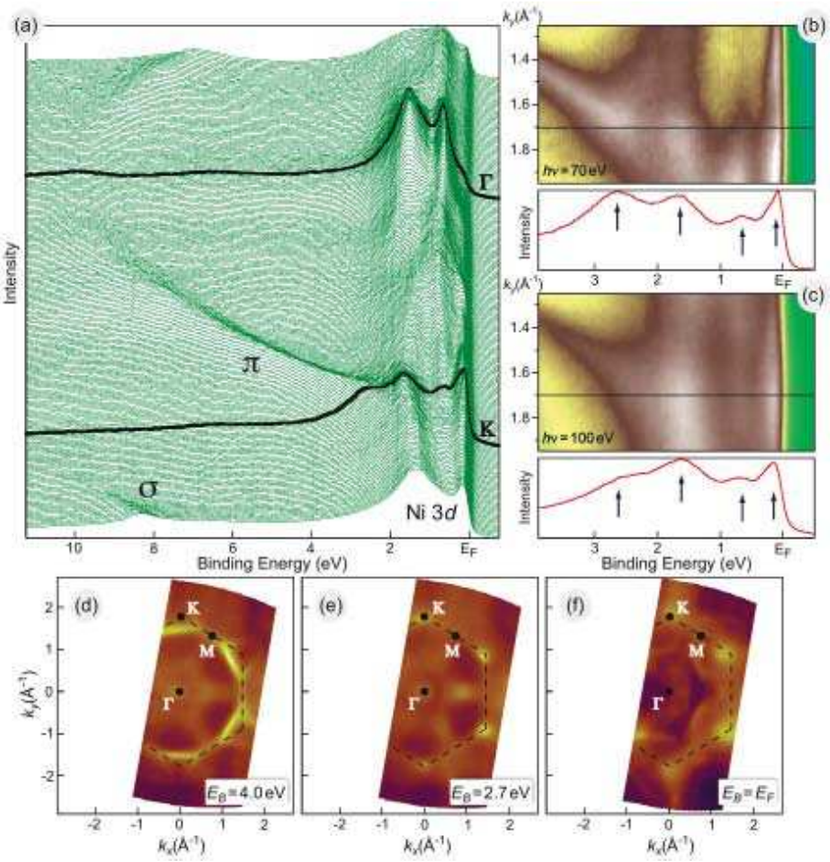

Fig. 9. (a) Series of the angle-resolved photoemission spectra of the graphene/Ni(111) system recorded along the $\Gamma - K$ direction of the hexagonal Brillouin zone at 100 eV of photon energy. Spectra corresponding to Γ and K points are marked by thick black lines. (b,c) Regions around the K point of photoemission intensity of the graphene/Ni(111) system measured at 70 eV and 100 eV of photon energy. The corresponding intensity profiles at the K point are shown in the lower panels with arrows indicating the main photoemission features discussed in the text. (d-f) Constant energy cuts of the 3D data sets in the energy-wave vector space at 4 eV, 2.7 eV of BE, and at E_F.

well-ordered structure of the graphene π-bands in the vicinity of the Fermi level and secondly, the Dirac-cone is not preserved. Both observations can be attributed to a strong interaction between graphene layer and metallic substrate leading to a strong hybridization between the graphene π and the Ni $3d$ valence band states. In the vicinity of the K point a number of photoemission peaks can be clearly distinguished: (i) a sharp peak about the Fermi level at $0.1 - 0.2$ eV BE, (ii) a graphene π-states-related peak at 2.65 eV BE, (iii) two peaks at 0.7 eV and 1.65 eV BE.

In the following we perform a detailed analysis of the experimentally obtained electronic structure relying on electronic structure calculations for the graphene/Ni(111) system discussed in Section 4. These calculations predict the existence of three interface hybrid states below the Fermi level originating from the strong hybridization between the Ni $3d$ and the graphene π states and corresponding to: (HS_1) bonding between C-fcc and interface Ni atoms; (HS_2) bonding between C-top and interface Ni atoms; (HS_3) antibonding between

C-fcc and interface Ni atoms. From the analysis of the experimental data in the region around the K point of the hexagonal Brillouin zone we could distinguish a number of flat bands, which are clearly separated from each other.

The interpretation of the experimentally observed photoemission features around the Fermi level could be performed as presented in the following. The photoemission peak close to the Fermi level (0.1-0.2 eV BE) could be considered as a combination of the interface hybrid state HS_3 (both spins) with a large contribution of the graphene π-character and the Ni $3d(\downarrow)$-band. The second peak at 0.7 eV BE could be assigned to the combination of the Ni $3d(\uparrow)$- and Ni $3d(\downarrow)$-bands present calculations. The feature at 1.65 eV could be considered as a combination of Ni $3d(\uparrow)$-band and $HS_2(\downarrow)$-state with a large graphene π-character. The last photoemission peak (2.65 eV BE) could be assigned to the interface hybrid state $HS_2(\uparrow)$ with large contribution of the graphene π-character.

In order to check the theoretical predictions concerning the spin-dependent electronic transport properties of the ideal graphene/Ni(111) interface, we perform a careful analysis of the constant energy photoemission maps close to the Fermi level. We would like to admit that such an analysis can be rather complicated due to the fact that Ni $3d$ bands, which dominate the photoemission intensity around the Fermi level, are very flat in the vicinity of E_F. Figure 9(d-f) shows the constant energy cuts of the 3D data set obtained at $h\nu$=100 eV for the graphene/Ni(111) system. These energy cuts were taken at (a) 4 eV and (b) 2.7 eV of BE as well as at (c) the Fermi level. The energy cut at $E_B = 4$ eV shows characteristic photoemission intensity patterns of the graphene layer, which reflect the symmetry of the system. Below the Dirac point (crossing of straight dispersion lines of π states in free-standing graphene) the graphene π bands are visible in the first Brillouin zone whereas no bands can be seen in the second one. Additionally several energy bands are present in the middle of the Brillouin zone, which also show hexagonal symmetry. These bands originate from the hybridization of the Ni and graphene valence band states. The constant energy cut taken in the region of the minimal binding energy of the graphene π states ($E_B = 2.7$ eV) is shown in Fig. 9(e). In the case of graphene/Ni(111) the Dirac point is not preserved due to the strong hybridization of Ni $3d$ and graphene π states around the K point. This can also be directly recognized at this energy cut where graphene π states produce broad intensity spots instead of sharp points in the wave-vector space. As in the previous case, we observe a number of valence band states in the middle part of the Brillouin zone, which again could be assigned to the hybridization-derived states.

The most interesting and important information in view on the spin-dependent transport properties of the graphene/Ni(111) system can be extracted form the constant energy cut obtained at the Fermi energy, which is presented in Fig. 9(f). Already the analysis of Fig. 9(a-c) shows that the photoemission intensity is increased around the K point and along the $\mathrm{K}-\mathrm{M}$ direction of the hexagonal Brillouin zone, that correlates with the increased photoemission intensity observed in the energy cut shown in Fig. 9(f) for the Fermi energy. Additionally, a number of arcs surrounding the K points and weak (but distinguished) diamond-shape regions of increased intensity is clearly visible in the middle part and around the M points of the Brillouin zone, respectively. Upon the comparison of the obtained photoemission results for the graphene/Ni(111) system [Fig. 9(a-f)] with the band structure calculations for this system (Section 4), we find very good agreement between theory and experiment. Particularly, the region around the Fermi level for the ideal graphene/Ni(111) system is well reproduced in the experiment, confirming the main predictions of the theory. Unfortunately, at the present

stage of the experiment, we can not specify the spin-character of energy bands, which should be the subject of future spin- and angle-resolved photoemission investigations.

6. Conclusions and outlook

In conclusion, the electronic structure and magnetic properties of the graphene/ferromagnet interface were investigated via combination of theoretical and experimental methods: DFT calculations, NEXAFS, XMCD, and mapping of the band structure by means of ARPES. From the theoretical side the different interfaces were analyzed: graphene/Ni(111), graphene/Co(0001), and graphene/1 ML Fe/Ni(111). Here the electronic structure of the interface as well as the effect of induced magnetism in graphene layer were discussed. In all cases a strong modification of the electronic structure of the graphene layer and FM substrate upon graphene adsorption were detected in theoretical calculations and confirmed by spectroscopic methods. This modification is due to the considerable hybridization of the graphene π and FM $3d$ valence band states accompanied by the partial charge transfer of spin-polarized electrons from FM onto C atoms leading to the appearance of the effective magnetic moment in the graphene layer. The presence of an effective magnetic moment on carbon atoms of the graphene layer was unambigously proven by XMCD and spin-resolved photoemission measurements for the graphene/Ni(111) system. The experimentally obtained electronic structure of occupied and unoccupied states of graphene/Ni(111) was compared with band structure calculations allowing the clear assignment of spectral features in the NEXAFS and ARPES data. The good agreement between theory and experiment was also found upon the analysis of the Fermi energy cuts, that give us an opportunity to confirm the main statements of the theoretical works predicting the spin-filtering effects of the graphene/Ni(111) interface. However, the clear assignment of the spectroscopic valence band features have to be performed in future spin-resolved photoemission experiments.

7. Acknowledgements

We would like to thank K. Horn, M. Weser, S. Böttcher, M. Fonin, and B. Paulus. We are also grateful to P. Kelly and L. Calmels for fruitful discussions. This work has been supported by the European Science Foundation (ESF) under the EUROCORES Programme EuroGRAPHENE (Project “SpinGraph”). E. V. appreciate the support from the German Research Foundation (DFG) through the Collaborative Research Center (SFB) 765 “Multivalency as chemical organisation and action principle: New architectures, functions and applications”. Y. D. acknowledges the financial support by the DFG under project DE 1679/2-1. We would like to acknowledge our co-workers in Max-lab (Lund) and BESSY (Berlin) synchrotron facilities for the technical assistance during experiment. We appreciate the support from the HLRN (High Performance Computing Network of Northern Germany) in Berlin.

8. References

Baberschke, K. (1996). The magnetism of nickel monolayers, *Appl. Phys. A* 62(5): 417–427.

Bae, S., Kim, H., Lee, Y., Xu, X., Park, J.-S., Zheng, Y., Balakrishnan, J., Lei, T., Kim, H. R., Song, Y. I., Kim, Y.-J., Kim, K. S., Ozyilmaz, B., Ahn, J.-H., Hong, B. H. & Iijima, S. (2010). Roll-to-roll production of 30-inch graphene films for transparent electrodes, *Nature Nanotech.* 5(8): 574–578.

Bertoni, G., Calmels, L., Altibelli, A. & Serin, V. (2005). First-principles calculation of the electronic structure and eels spectra at the graphene/Ni(111) interface, *Phys. Rev. B* 71(7): 075402 1–8.

Blochl, P. (1994). Projector augmented-wave method, *Phys. Rev. B* 50(24): 17953–17979.

Boukhvalov, D. W. & Katsnelson, M. I. (2009). Chemical functionalization of graphene, *J. Phys.: Condens. Matter.* 21(34): 344205 1–12.

Brako, R., Sokcevic, D., Lazic, P. & Atodiresei, N. (2010). Graphene on Ir(111) surface: From van der Waals to strong bonding, *arXiv:1006.1280v1 [cond-mat.mes-hall]*. URL: *http://arxiv.org/abs/1006.1280*.

Carra, P., Thole, B., Altarelli, M. & Wang, X. (1993). X-ray circular-dichroism and local magnetic-fields, *Phys. Rev. Lett.* 70(5): 694–697.

Céspedes, O., Ferreira, M. S., Sanvito, S., Kociak, M. & Coey, J. M. D. (2004). Contact induced magnetism in carbon nanotubes, *J. Phys.: Condens. Matter.* 16: L155–L161.

Coletti, C., Riedl, C., Lee, D. S., Krauss, B., Patthey, L., von Klitzing, K., Smet, J. H. & Starke, U. (2010). Charge neutrality and band-gap tuning of epitaxial graphene on SiC by molecular doping, *Phys. Rev. B* 81(23): 235401 1–8.

Coraux, J., N'Diaye, A. T., Busse, C. & Michely, T. (2008). Structural coherency of graphene on Ir(111), *Nano Lett.* 8(2): 565–570.

Coraux, J., N'Diaye, A. T., Engler, M., Busse, C., Wall, D., Buckanie, N., zu Heringdorf, F.-J. M., van Gastel, R., Poelsema, B. & Michely, T. (2009). Growth of graphene on Ir(111), *New J. Phys.* 11(2): 023006 1–22.

Dedkov, Y. S. & Fonin, M. (2010). Electronic and magnetic properties of the graphene-ferromagnet interface, *New J. Phys. (accepted)* .

Dedkov, Y. S., Fonin, M. & Laubschat, C. (2008). A possible source of spin-polarized electrons: The inert graphene/Ni(111) system, *Appl. Phys. Lett.* 92(5): 052506 1–3.

Dedkov, Y. S., Fonin, M., Rüdiger, U. & Laubschat, C. (2008a). Graphene-protected iron layer on Ni(111), *Appl. Phys. Lett.* 93(2): 022509 1–3.

Dedkov, Y. S., Fonin, M., Rüdiger, U. & Laubschat, C. (2008b). Rashba effect in the graphene/Ni(111) system, *Phys. Rev. Lett.* 100(10): 107602 1–4.

Dedkov, Y. S., Shikin, A. M., Adamchuk, V. K., Molodtsov, S. L., Laubschat, C., Bauer, A. & Kaindl, G. (2001). Intercalation of copper underneath a monolayer of graphite on Ni(111), *Phys. Rev. B* 64(3): 035405 1–6.

Dedkov, Y., Vyalikh, D., Holder, M., Weser, M., Molodtsov, S., Laubschat, C., Kucherenko, Y. & Fonin, M. (2008). Dispersion of 4f impurity states in photoemission spectra of Yb/W(110), *Phys. Rev. B* 78(15): 153404 1–4.

Dhesi, S., Dürr, H., van der Laan, G., Dudzik, E. & Brookes, N. (1999). Electronic and magnetic structure of thin Ni films on Co/Cu(001), *Phys. Rev. B* 60(18): 12852–12860.

Dion, M., Rydberg, H., Schroder, E., Langreth, D. & Lundqvist, B. (2004). Van der Waals density functional for general geometries, *Phys. Rev. Lett.* 92(24): 246401 1–4.

Dutta, S. & Pati, S. K. (2008). Half-metallicity in undoped and boron doped graphene nanoribbons in the presence of semilocal exchange-correlation interactions, *J. Phys. Chem. B* 112(5): 1333–1335.

Enderlein, C., Kim, Y. S., Bostwick, A., Rotenberg, E. & Horn, K. (2010). The formation of an energy gap in graphene on ruthenium by controlling the interface, *New J. Phys.* 12: 033014 1–9.

Eom, D., Prezzi, D., Rim, K. T., Zhou, H., Lefenfeld, M., Xiao, S., Nuckolls, C., Hybertsen, M. S., Heinz, T. F. & Flynn, G. W. (2009). Structure and electronic properties of graphene nanoislands on Co(0001), *Nano. Lett.* 9(8): 2844–2848.

Fuentes-Cabrera, M., Baskes, M. I., Melechko, A. V. & Simpson, M. L. (2008). Bridge structure for the graphene/Ni(111) system: A first principles study, *Phys. Rev. B* 77(3): 1–5.

Gamo, Y., Nagashima, A., Wakabayashi, M., Terai, M. & Oshima, C. (1997). Atomic structure of monolayer graphite formed on Ni(111), *Surf. Sci.* 374(1-3): 61–64.

Geim, A. (2009). Graphene: Status and prospects, *Science* 324(5934): 1530–1534.

Geim, A. K. & Novoselov, K. S. (2007). The rise of graphene, *Nature Mater.* 6: 183–191.

Gierz, I., Riedl, C., Starke, U., Ast, C. & Kern, K. (2008). Atomic hole doping of graphene, *Nano Lett.* 8(12): 4603–4607.

Gierz, I., Suzuki, T., Weitz, R. T., Lee, D. S., Krauss, B., Riedl, C., Starke, U., Hoechst, H., Smet, J. H., Ast, C. R. & Kern, K. (2010). Electronic decoupling of an epitaxial graphene monolayer by gold intercalation, *Phys. Rev. B* 81(23): 235408 1–6.

Grimme, S. (2004). Accurate description of van der waals complexes by density functional theory including empirical corrections, *J. Comput. Chem.* 25(12): 1463–1473.

Grüneis, A. & Vyalikh, D. (2008). Tunable hybridization between electronic states of graphene and a metal surface, *Phys. Rev. B* 77(19): 193401 1–4.

Hu, Z., Ogletree, D., van Hove, M. & Somorjai, G. (1987). LEED theory for incommensurate overlayers - application to graphite on Pt(111), *Surf. Sci.* 180(2-3): 433–459.

Huang, D., Jeng, H., Chang, C., Guo, G., Chen, J., Wu, W., Chung, S., Shyu, S., Wu, C., Lin, H. & Chen, C. (2002). Orbital magnetic moments of oxygen and chromium in CrO_2, *Phys. Rev. B* 66(17): 174440 1–5.

Karpan, V. M., Giovannetti, G., Khomyakov, P. A., Talanana, M., Starikov, A. A., Zwierzycki, M., van den Brink, J., Brocks, G. & Kelly, P. J. (2007). Graphite and graphene as perfect spin filters, *Phys. Rev. Lett.* 99(17): 176602 1–4.

Karpan, V. M., Khomyakov, P. A., Starikov, A. A., Giovannetti, G., Zwierzycki, M., Talanana, M., Brocks, G., Brink, J. V. D. & Kelly, P. J. (2008). Theoretical prediction of perfect spin filtering at interfaces between close-packed surfaces of Ni or Co and graphite or graphene, *Phys. Rev. B* 78(19): 1–11.

Kim, K. S., Zhao, Y., Jang, H., Lee, S. Y., Kim, J. M., Kim, K. S., Ahn, J.-H., Kim, P., Choi, J.-Y. & Hong, B. H. (2029). Large-scale pattern growth of graphene films for stretchable transparent electrodes, *Nature* 457(7230): 706–710.

Klink, C., Stensgaard, I., Besenbacher, F. & Lægsgaard, E. (1995). An STM study of carbon-induced structures on Ni(111) - evidence for a carbidic-phase clock reconstruction, *Surf. Sci.* 342(1-3): 250–260.

Kresse, G. & Furthmuller, J. (1996a). Efficiency of ab-initio total energy calculations for metals and semiconductors using a plane-wave basis set, *Comp. Mater. Sci.* 6(1): 15–50.

Kresse, G. & Furthmuller, J. (1996b). Efficient iterative schemes for ab initio total-energy calculations using a plane-wave basis set, *Phys. Rev. B* 54(16): 11169–11186.

Land, T., Michely, T., Behm, R., Hemminger, J. & Comsa, G. (1992). STM investigation of single layer graphite structures produced on Pt(111) by hydrocarbon decomposition, *Surf. Sci.* 264(3): 261–270.

Mao, Y., Yuan, J. & Zhong, J. (2008). Density functional calculation of transition metal adatom adsorption on graphene, *J. Phys.: Condens. Matter.* 20(11): 115209 1–6.

Martoccia, D., Willmott, P. R., Brugger, T., Bjorck, M., Gunther, S., Schleputz, C. M., Cervellino, A., Pauli, S. A., Patterson, B. D., Marchini, S., Wintterlin, J., Moritz, W. & Greber, T.

(2008). Graphene on Ru(0001): A 25 × 25 supercell, *Phys. Rev. Lett.* 101(12): 126102 1–4.

Mertins, H., Valencia, S., Gudat, W., Oppeneer, P., Zaharko, O. & Grimmer, H. (2004). Direct observation of local ferromagnetism on carbon in C/Fe multilayers, *Europhys. Lett.* 66: 743–748.

Morozov, S. V., Novoselov, K. S., Katsnelson, M. I., Schedin, F., Elias, D. C., Jaszczak, J. A. & Geim, A. K. (2008). Giant intrinsic carrier mobilities in graphene and its bilayer, *Phys. Rev. Lett.* 100(1): 016602 1–4.

Nagashima, A., Itoh, H., Ichinokawa, T., Oshima, C. & Otani, S. (1994). Change in the electronic states of graphite overlayers depending on thickness, *Phys. Rev. B* 50(7): 4756–4763.

Nagashima, A., Tejima, N. & Oshima, C. (1994). Electronic states of the pristine and alkali-metal-intercalated monolayer graphite/Ni(111) systems, *Phys. Rev. B* 50(23): 17487–17495.

N'Diaye, A., Bleikamp, S., Feibelman, P. & Michely, T. (2006). Two-dimensional Ir cluster lattice on a graphene moiré on Ir(111), *Phys. Rev. Lett.* 97(21): 215501 1–4.

Nesvizhskii, A., Ankudinov, A., Rehr, J. & Baberschke, K. (2000). Interpretation of x-ray magnetic circular dichroism and x-ray absorption near-edge structure in Ni, *Phys. Rev. B* 62(23): 15295–15298.

Neto, A. C., Guinea, F., Peres, N., Novoselov, K. & Geim, A. (2009). The electronic properties of graphene, *Rev. Mod. Phys.* 81(1): 109–162.

Novoselov, K., Geim, A., Morozov, S., Jiang, D., Katsnelson, M., Grigorieva, I., Dubonos, S. & Firsov, A. (2005). Two-dimensional gas of massless dirac fermions in graphene, *Nature* 438(7065): 197–200.

Paulus, B. & Rosciszewski, K. (2009). Application of the method of increments to the adsorption of h2s on graphene, *Int. J. Quantum. Chem.* 109(13): 3055–3062.

Perdew, J., Burke, K. & Ernzerhof, M. (1996). Generalized gradient approximation made simple, *Phys. Rev. Lett.* 77(18): 3865–3868.

Pisani, C., Maschio, L., Casassa, S., Halo, M., Schuetz, M. & Usvyat, D. (2008). Periodic local MP2 method for the study of electronic correlation in crystals: Theory and preliminary applications, *J. Comput. Chem.* 29(13): 2113–2124.

Preobrajenski, A. B., Ng, M. L., Vinogradov, A. S. & Mårtensson, N. (2008). Controlling graphene corrugation on lattice-mismatched substrates, *Phys. Rev. B* 78(7): 073401 1–4.

Rosei, R., Decresceni, M., Sette, F., Quaresima, C., Savoia, A. & Perfetti, P. (1983). Structure of graphitic carbon on Ni(111) - a surface extended-energy-loss fine-structure study, *Phys. Rev. B* 28(2): 1161–1164.

Rusz, J., Preobrajenski, A. B., Ng, M. L., Vinogradov, N. A., Mårtensson, N., Wessely, O., Sanyal, B. & Eriksson, O. (2010). Dynamical effects in x-ray absorption spectra of graphene and monolayered h-BN on Ni(111), *Phys. Rev. B* 81(7): 073402 1–4.

Sasaki, M., Yamada, Y., Ogiwara, Y., Yagyu, S. & Yamamoto, S. (2000). Moire contrast in the local tunneling barrier height images of monolayer graphite on Pt(111), *Phys. Rev. B* 61(23): 15653–15656.

Schedin, F., Geim, A. K., Morozov, S. V., Hill, E. W., Blake, P., Katsnelson, M. I. & Novoselov, K. S. (2007). Detection of individual gas molecules adsorbed on graphene, *Nature Mater.* 6(9): 652–655.

Shikin, A., Prudnikova, G., Adamchuk, V., Moresco, F. & Rieder, K. (2000). Surface intercalation of gold underneath a graphite monolayer on Ni(111) studied by angle-resolved photoemission and high-resolution electron-energy-loss spectroscopy, *Phys. Rev. B* 62(19): 13202–13208.

Sorg, C., Ponpandian, N., Bernien, M., Baberschke, K., Wende, H. & Wu, R. Q. (2006). Induced magnetism of oxygen in surfactant-grown Fe, Co, and Ni monolayers, *Phys. Rev. B* 73(6): 064409 1–7.

Sorg, C., Ponpandian, N., Scherz, A., Wende, H., Nunthel, R., Gleitsmann, T. & Baberschke, K. (2004). The magnetism of ultrathin Ni films grown with O surfactant, *Surf. Sci.* 565(2-3): 197–205.

Srivastava, P., Wilhelm, F., Ney, A., Farle, M., Wende, H., Haack, N., Ceballos, G. & Baberschke, K. (1998). Magnetic moments and curie temperatures of Ni and Co thin films and coupled trilayers, *Phys. Rev. B* 58(9): 5701–5706.

Stöhr, J. (1999). Exploring the microscopic origin of magnetic anisotropies with x-ray magnetic circular dichroism (xmcd) spectroscopy, *J. Magn. Magn. Mat.* 200(1): 470–497.

Stöhr, J. & Samant, M. (1999). Liquid crystal alignment by rubbed polymer surfaces: a microscopic bond orientation model, *J. Electr. Spectr. Rel. Phenom.* 98-99: 189–207.

Sutter, P., Hybertsen, M. S., Sadowski, J. T. & Sutter, E. (2009). Electronic structure of few-layer epitaxial graphene on Ru(0001), *Nano Lett.* 9(7): 2654–60.

Thole, B., Carra, P., Sette, F. & van der Laan, G. (1992). X-ray circular-dichroism as a probe of orbital magnetization, *Phys. Rev. Lett.* 68(12): 1943–1946.

Tombros, N., Jozsa, C., Popinciuc, M., Jonkman, H. T. & van Wees, B. J. (2007). Electronic spin transport and spin precession in single graphene layers at room temperature, *Nature* 448(7153): 571–574.

Wang, B., Bocquet, M. L., Marchini, S., Guenther, S. & Wintterlin, J. (2008). Chemical origin of a graphene moire overlayer on Ru(0001), *Phys. Chem. Chem. Phys.* 10(24): 3530–3534.

Wang, X., Li, X., Zhang, L., Yoon, Y., Weber, P. K., Wang, H., Guo, J. & Dai, H. (2009). N-doping of graphene through electrothermal reactions with ammonia, *Science* 324(5928): 768–771.

Wintterlin, J. & Bocquet, M. L. (2009). Graphene on metal surfaces, *Surf. Sci.* 603(10-12): 1841–1852.

Yamamoto, K., Fukishima, M., Osaka, T. & Oshima, C. (1992). Charge-transfer mechanism for the (monolayer graphite)-Ni(111) system, *Phys. Rev. B* 45(19): 11358–11361.

Yazyev, O. V. & Pasquarello, A. (2009). Magnetoresistive junctions based on epitaxial graphene and hexagonal boron nitride, *Phys. Rev. B* 80(3): 035408 1–5.

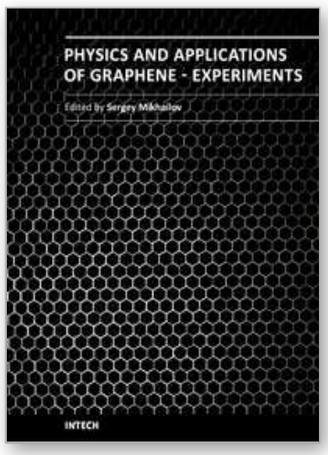

Physics and Applications of Graphene - Experiments

Edited by Dr. Sergey Mikhailov

ISBN 978-953-307-217-3
Hard cover, 540 pages
Publisher InTech
Published online 19, April, 2011
Published in print edition April, 2011

The Stone Age, the Bronze Age, the Iron Age... Every global epoch in the history of the mankind is characterized by materials used in it. In 2004 a new era in material science was opened: the era of graphene or, more generally, of two-dimensional materials. Graphene is the strongest and the most stretchable known material, it has the record thermal conductivity and the very high mobility of charge carriers. It demonstrates many interesting fundamental physical effects and promises a lot of applications, among which are conductive ink, terahertz transistors, ultrafast photodetectors and bendable touch screens. In 2010 Andre Geim and Konstantin Novoselov were awarded the Nobel Prize in Physics "for groundbreaking experiments regarding the two-dimensional material graphene". The two volumes Physics and Applications of Graphene - Experiments and Physics and Applications of Graphene - Theory contain a collection of research articles reporting on different aspects of experimental and theoretical studies of this new material.

INTECH
open science | open minds

InTech Europe
University Campus STeP Ri
Slavka Krautzeka 83/A
51000 Rijeka, Croatia
Phone: +385 (51) 770 447
Fax: +385 (51) 686 166
www.intechopen.com

InTech China
Unit 405, Office Block, Hotel Equatorial Shanghai
No.65, Yan An Road (West), Shanghai, 200040, China
中国上海市延安西路65号上海国际贵都大饭店办公楼405单元
Phone: +86-21-62489820
Fax: +86-21-62489821

IntechOpen